Submitted to *J. Geophys. Res. Atm.*, November 5, 2002.

Mineral dust and global tropospheric chemistry: Relative roles of photolysis and heterogeneous uptake

Huisheng Bian and Charles S. Zender

Department of Earth System Science, University of California at Irvine

Abstract. We investigate the influence of mineral dust on tropospheric chemistry in the present climate at the global scale. The analysis examines the effects of dust on photochemistry and heterogeneous uptake, operating independently and together. In numerical experiments the size-resolved, time-varying mineral dust distribution predicted by the global Dust Entrainment And Deposition (DEAD) model perturbs the gas phase species in a global Chemical Transport Model (UCI CTM). We find that the photolysis perturbation dominates limited regions in the low to middle troposphere, while heterogeneous uptake dominates the rest of atmosphere (H_2O_2 is an exception). Coupling of the photochemical and heterogeneous effects of dust is weak in the global mean but significant in dusty regions, where coupling is sometimes responsible for more than 50% of local O_3 changes. Ozone and odd-nitrogen concentrations are perturbed in opposite directions by photolysis and heterogeneous chemistry, resulting in a weak net change. However, both processes decrease the concentrations of OH and HO_2. The global mean change due to dust is -0.7% for tropospheric O_3, -11.1% for OH, -5.2% for HO_2, and -3.5% for HNO_3. Large seasonal signals are present near dust source regions. Over the north African region and tropical Atlantic Ocean downwind, OH decreases by -66.8%, a factor of six more than global mean value. In polar regions, O_3 change is dominated by transported O_3 and is not sensitive to local dust concentration. O_3 change due to photochemistry is not only sensitive to dust vertical structure in dusty regions, but also depends on the availability of O_3 precursors. O_3 change due to heterogeneous reactions on dust is sensitive to dust vertical structure, mainly through the influence of temperature on uptake rates.

1. Introduction

Aerosols impact the chemical composition of the atmosphere by providing a surface for heterogeneous chemistry, and for light scattering and absorption at photolytic wavelengths. Mineral dust is an important aerosol to consider in atmospheric chemistry because its natural and anthropogenic sources account for one-third to one-half of total annual aerosol emissions by mass [*Penner et al.*, 2001]. Moreover, dust emissions are sensitive to land use change [*Tegen and Fung*, 1995] and to long term climate variations [*Ram and Koenig*, 1997], so its atmospheric abundance varies on many timescales. This work focuses on the current annual mean and seasonal cycle of global dust-chemistry interactions.

Convincing evidence that heterogeneous chemistry on mineral dust significantly alters the concentration of important atmospheric gases has been firmly established in field, lab, and model settings [*Zhang et al.*, 1994; *Dentener et al.*, 1996; *Tabazadeh et al.*, 1998; *Zhang and Carmichael*, 1999; *Goodman et al.*, 2000; *Galy-Lacaus et al.*, 2002; *Underwood et al.*, 2002; *Michel et al.*, 2002]. Research also shows mineral dust significantly alters atmospheric photochemistry by absorption and scattering in photolytic wavelengths [*Dickerson et al.*, 1997; *Jacobson*, 1998; *He and Carmichael*, 1999; *Balis et al.*, 2001; *Bian et al.*, 2002]. However, definitive answers to the global scale influence of dust on atmospheric

chemistry are evasive because of uncertainties in the spatial and temporal distribution of dust, and its mineral, optical, and chemical properties [e.g., *Sokolik et al.*, 2001].

Previous three-dimensional Chemical Transport Model (CTM) simulations of the influence of dust on chemistry focus on the impact of one process (photochemical or heterogeneous), in isolation, on atmospheric oxidants. Furthermore, many of these efforts were conducted on regional spatial scales and/or event-based or synoptic timescales. We investigate in this paper the chemical alteration of the troposphere by both photochemical forcing and heterogeneous uptake due to dust in a CTM framework. To our knowledge, this is the first attempt to integrate and compare both processes at the global and annual scale.

Our objectives are: (1) Estimate the perturbation by dust to global oxidant distributions due to the coupled effects of photolysis and heterogeneous uptake, (2) Isolate the effect of each process and learn whether there are non-linear interactions between them, (3) Identify regions and seasons where dust has its maximum influence on chemistry, (4) Understand the influence of dust horizontal and vertical distributions on ozone production.

The paper is organized as follows. Section 2 describes the two global models employed. Section 3 presents, in order, the results of the model simulations of the photochemical, heterogeneous uptake, and coupled effects of dust, and concludes with the effects of spatial distribution in selected regions. We discuss our main findings, their uncertainties, and implications for future studies follows in Section 4.

2. Simulation Framework

2.1. CTM description

The UCI CTM [*Wild and Akimoto*, 2001] includes a detailed tropospheric photochemical scheme which uses the ASAD scheme [*Carver et al.*, 1997] with an implicit solver. The chemical scheme includes complete treatment of inorganic plus methane chemistry and a lumped "family" treatment of hydrocarbon oxidation schemes for the representative species butane, propane, xylene and isoprene. This tropospheric O_3-NO_x-NMHC chemistry scheme contains 36 species, with 88 chemical reactions and 22 photochemical reactions [*Wild and Prather*, 2000; *Bian and Prather*, 2002]. Reaction rates are principally taken from *DeMore et al.* [1997] and from *Atkinson et al.* [1997], with additional rates from [*Hough*, 1991] and from the Leeds University Master Chemical Mechanism. Photolysis rates are calculated with an on-line treatment of molecular, aerosol, and water and ice cloud absorption and scattering using the Fast-J scheme [*Wild et al.*, 2000; *Bian and Prather*, 2002]. For use in calculating photolysis rates, stratospheric ozone is taken from the Models and Measurements (M&M) climatology [*Park et al.*, 1999] while tropospheric ozone is taken from the instantaneous CTM values.

The meteorology driving the CTM is provided by the Goddard Institute for Space Studies (GISS) general circulation model version II′ ($4^\circ \times 5^\circ$, 9 vertical layers) based on the climatological sea surface temperature of the 1980s. The meteorological fields are supplied every 3 hours and linearly interpolated to the nearest time step. The advection scheme conserves second-order moments and considers not only gradients of tracer concentration but also the curvature in the tracer distribution [*Prather*, 1986].

Dry deposition is treated with a resistance-in-series scheme based on the surface meteorological properties, vegetation type and species solubility. Wet deposition of soluble species is allowed for during convective transport and in large-scale precipitation using Henry's Law coefficients. Washout in rainfall uses precipitation mass fluxes from the supplied meteorological data and the pH of the water droplets. Evaporation occurring in the lower atmosphere allows these processes to transport soluble trace gases down through the atmosphere rather than removing them entirely.

We map the GEIA inventories of trace species emissions from $1^\circ \times 1^\circ$ resolution to the model grid, preserving the second order moments of the emissions. Additional emissions for CO and biomass burning sources at $4^\circ \times 5^\circ$ resolution are from *Wang et al.* [1998a]. Diurnal variations are provided for industrial and biogenic sources, and seasonal variations are provided for soil emissions, methane, and biomass burning sources. NO from lightning is based on the parameterization of *Price and Rind* [1992]. The vertical mass flux from the meteorological fields is used to define deep convective events to distribute the NO source. An NO source from aircraft is also included [*Baughcum et al.*, 1996].

The upper boundary for stratospheric ozone is calculated with the Synoz model [*McLinden et al.*, 2000]. The global annual mean flux of ozone from the stratosphere is specified as 475 Tg yr^{-1} based on observations [*Murphy and Fahey*, 1994]. Synoz allows the circulation to determine where and when O_3 enters the troposphere. A dynamical tropopause is diagnosed as the 120 ppb isopleth of this synthetic ozone. Below this level, the tropospheric chemistry scheme is applied, and above, a simplified stratospheric scheme is used.

2.2. Mineral Dust

The usefulness of global chemical studies of mineral dust depends, in part, on the fidelity of the simulated dust distribution to observations. The climatological global 3-D dust concentrations used in the UCI CTM are predicted

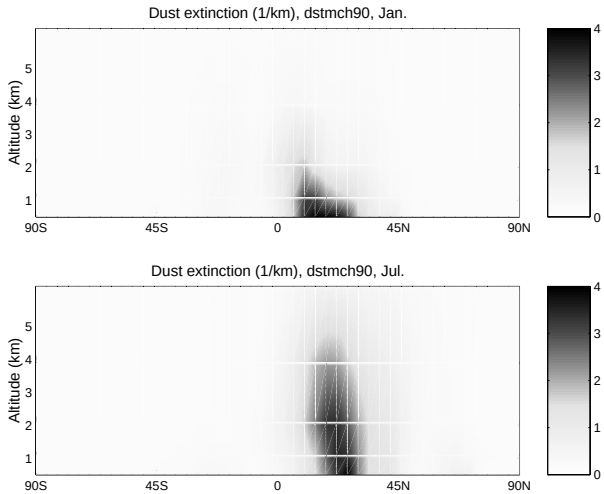

Figure 1. Zonal mean dust extinction [km^{-1}] at 630 nm in (a) January and (b) July.

by the mineral Dust Entrainment And Deposition (DEAD) model [*Zender et al.*, 2002]. Predictions from DEAD have been used and evaluated against field measurements in numerous aerosol studies [*Rasch et al.*, 2001; *Collins et al.*, 2001, 2002; *Mahowald et al.*, 2002; *Luo et al.*, 2002; *Zender et al.*, 2002].

DEAD predicts the size-resolved distribution of atmospheric dust in four size bins (0.1–1, 1–2.5, 2.5–5, and 5–10 μm). Mobilization processes include entrainment thresholds, moisture inhibition, drag partitioning, saltation feedback, and erodibility enhancements in sedimentary basins. Dry deposition processes include sedimentation and turbulent mix-out. Nucleation and collision scavenging in both stratiform and convective cloud types are simulated. DEAD simulations of 1994–1998 [*Zender et al.*, 2002] in the NCAR MATCH model [*Rasch et al.*, 1997] at T62$\times$L28 resolution were averaged to create global 3-D monthly mean dust concentrations for the UCI CTM. These dust concentrations are then re-gridded to the spatial and temporal resolution of the UCI CTM.

Figure 1 depicts the predicted zonal mean mineral dust extinction [km^{-1}] at 630 nm in January and July. Strong summertime convection lifts dust into higher atmosphere in July, and spreads more dust into remote region. Dust centers around $10°$N in January and shifts north to $20°$N in July. The annual mean atmospheric dust burden is 29 mg m^{-2}. The geographic and seasonal variations of dust loading are shown and evaluated in *Zender et al.* [2002] and *Luo et al.* [2002].

3. Results and Discussions

The results presented are taken from the final 12 months of CTM simulations of July 1 of year 1 through Jan 31 of year 3. These nineteen month runs include a seven-month spin-up time which allows for most chemically important trace gases, except CH_4, to reach steady state. Throughout this paper, the influence of dust on atmospheric chemistry is isolated by subtracting the control run (without aerosol) from the perturbation run (with dust) and (for some quantities) dividing by the control run. The species changes reported refer only to tropospheric (i.e., not tropospheric + stratospheric) abundances.

3.1. Effects of Photochemical Forcing

Aerosols manipulate the atmospheric radiance field in such an intricate way that outstanding problems remain in modeling the closure of even the clear sky radiative budget [*Valero et al.*, 2002]. *Sokolik et al.* [2001] review current experimental and theoretical approaches used to quantify the dust radiative effects. They point out that despite recent advances, dust optical properties remain poorly quantified due to limited data and incomplete understanding of relevant physical and chemical properties. The reader is referred to the existing literature on the sensitivity of photochemistry to plausible ranges of dust optical properties [*Liao and Seinfeld*, 1998; *He and Carmichael*, 1999].

The refractive index n is an essential parameter required to derive the optical properties used in photolysis rate calculations. Specifically, Fast-J requires the single scattering albedo and the first 7 coefficients in the Legendre expansion of the scattering phase function for ultraviolet and visible wavelengths (300–600 nm) [*Wild et al.*, 2000; *Bian and Prather*, 2002]. As in *Bian et al.* [2002], we use $n = 1.50 + 0.025\mathrm{i}$ which is approximately the mean value of measurements by *Patterson* [1981] between 300–400 nm. For the lognormally distributed long range transport mode of dust with volume median diameter of 2.5 μm [*Zender et al.*, 2002], the single scattering albedo at $\lambda = 300$ nm is 0.64. Previous observations and simulations agree that dust causes significant absorption in the key tropospheric photochemical wavelengths (300–400 nm) [*Savoie et al.*, 2000; *Diaz et al.*, 2001; *Kaufman et al.*, 2001; *Dubovik et al.*, 2002]. The influence of Relative Humidity (RH) on n is neglected since the radiative properties of atmospheric dust are relatively insensitive to RH changes [*Li-Jones et al.*, 1998; *He and Carmichael*, 1999].

Plate 1 and Figure 2 show the effects of photolysis alteration by dust on the O_3 and OH fields in January and July, respectively. We show only O_3 and OH because they represent the key tropospheric oxidants and drive tropo-

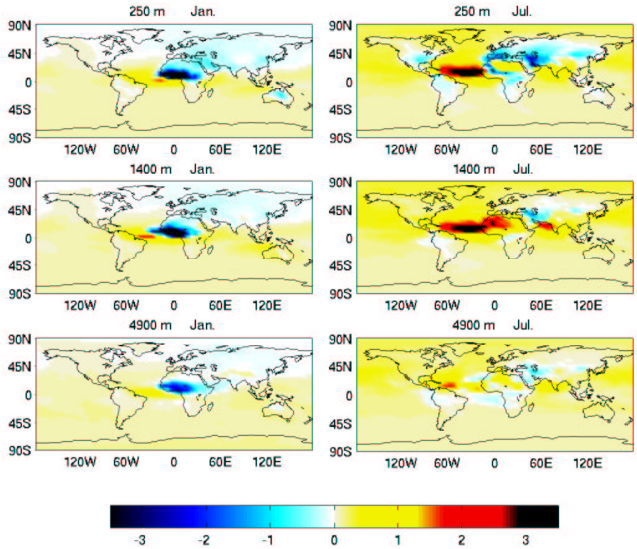

Plate 1. Photolysis perturbation to O_3 [ppb] by dust in January and July at three atmospheric layers.

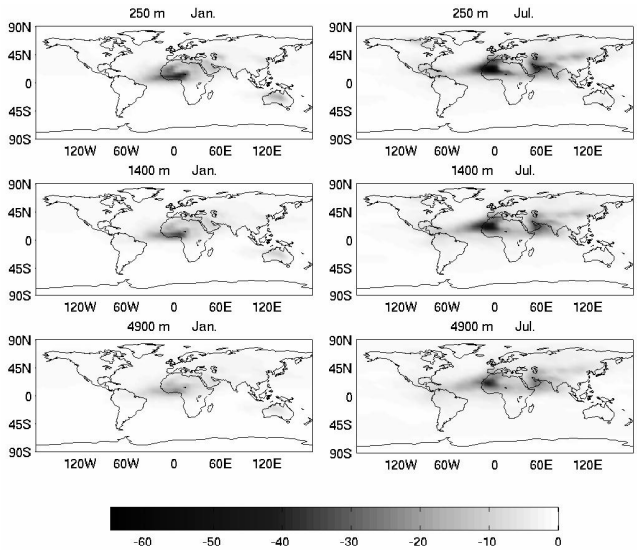

Figure 2. Photolysis perturbation to OH [%] by dust in January and July at three atmospheric layers.

spheric chemistry. The maximum perturbations are in dust source regions in the boundary layer and decrease with altitude. The perturbation patterns are consistent with dust abundance, and show that tropospheric chemistry responds quickly to photochemical forcing. January is characterized by decreased O_3 at all levels in the African dust region,

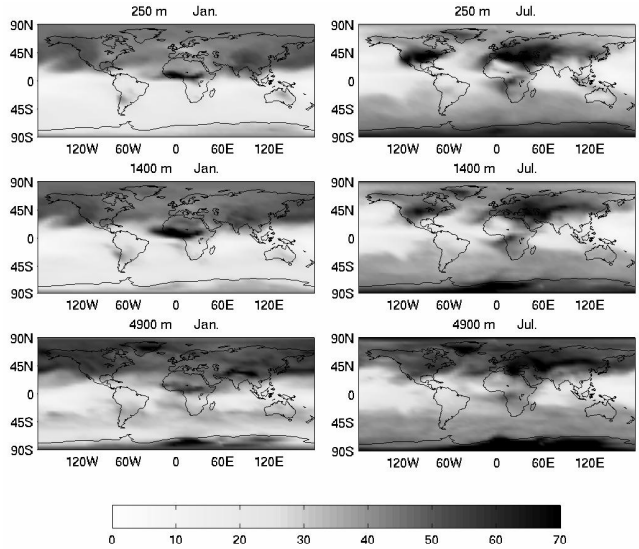

Figure 3. Unperturbed climatological O_3 [ppb] in January and July at three atmospheric layers simulated by gas phase chemistry alone.

while a more diffuse O_3 decrease occurs over Asia. In July, there is a striking change in the sign of the O_3 perturbation due to African dust. The Asian dust O_3 perturbation also changes from decreasing to increasing above the boundary layer.

To help explain this response, we show the unperturbed O_3 abundance in Figure 3. Seasonal biomass burning forms the O_3 maxima in sub-Saharan Africa. Comparison of Plate 1 and Figure 3 shows that in both January and July the maximum O_3 reduction by dust occurs over continental, high-NO_x, ozone-producing regions. Previous studies show that over low-NO_x oceanic regions, photochemistry destroys O_3 [*Olson et al.*, 1997]. Dust absorption reduces photochemistry, and hence this loss, in low-NO_x oceanic regions. This causes O_3 to increase there[*Bian et al.*, 2002]. The increased O_3 perturbation in remote regions in July is associated with more background dust and more active chemistry in northern summer.

The tropical Atlantic ocean is an area of particular interest because of its proximity to dust sources. Here the O_3 change is small in January, and increases by more than 3 ppb in July. The nearby upstream dust sources and biomass burning emissions (which provide high-NO_x) are controlling factors in this seasonal change. Biomass burning in the Sahel in January (Figure 3) is close to dust emissions and transport paths in north Africa (Figure 5 of *Zender et al.* [2002]). However, the centers of dust and biomass burning emissions

Table 1. January, July, and Annual mean photochemical perturbation [%] by dust of NH, SH, and Global O_3 and OH.

Region	O_3			OH		
	Jan	Jul	Ann.	Jan	Jul	Ann.
NH	-0.12	0.98	0.19	-2.51	-4.82	-4.07
SH	0.40	0.21	0.26	-0.68	-1.03	-0.82
Global	0.14	0.59	0.23	-1.59	-2.92	-2.44

are both shifted by about 10° in opposite directions in July. This leaves low-NO_x in the tropical North Atlantic ocean in July. These results are consistent with previous studies which show that absorbing aerosol reduces ground level O_3 in polluted environments [*Dickerson et al.*, 1997; *Jacobson*, 1998; *He and Carmichael*, 1999] and that O_3 increases or decreases in the upper atmosphere depending on the availability of NO_x [*He and Carmichael*, 1999]. The OH decreases in Figure 2 are consistent with the spatial distribution of dust (Figure 5 in *Zender et al.* [2002]). The decreases are driven by reductions in $O(^1D)$ caused by reduced ultraviolet photolysis of O_3. The OH decreases are exacerbated by chemical reduction of OH due to reduced NO and increased CO due to photolysis changes [*Bian et al.*, 2002].

Table 1 lists the mean January, July and annual changes in O_3 [%] and OH [%] due to light scattering and absorption by dust. The amplitude of the O_3 perturbation in the Northern Hemisphere (NH) is much larger than the Southern Hemisphere (SH) perturbation. This is due to the three factors, absolute dust amount, proximity to O_3 precursors, and reflective land area, already mentioned. The global annual mean perturbation of O_3 and OH by dust via photolysis is 0.23% and -2.44%, respectively. The global O_3 perturbation is a factor of four larger in July than in January. The perturbation of both gases is about a factor of four larger in the NH than in the SH in both seasons and in the annual mean (for OH). The annual change in O_3 is about 0.2% in each hemisphere, because the seasonal changes differ dramatically.

3.2. Effects of Heterogeneous Uptake

Direct measurements and theoretical research provide convincing evidence that mineral dust plays important roles in altering atmospheric chemistry through heterogeneous reactions [*Goodman et al.*, 2000; *Galy-Lacaus et al.*, 2002]. Once sequestered on mineral dust particles, oxidants such as HNO_3 and SO_2 appear to undergo fast neutralization reactions with alkaline material (e.g., $CaCO_3$) in mineral dust [*Dentener et al.*, 1996; *Zhang and Carmichael*, 1999; *Underwood et al.*, 2002; *Michel et al.*, 2002]. *Dentener et al.* [1996] estimated that at least 40% of total column nitrate is found on the mineral aerosol over vast regions of the NH. We simulate the net direct uptake on mineral dust of O_3, odd-hydrogen (OH, HO_2), odd-nitrogen (NO_2, NO_3, and HNO_3), N_2O_5, and H_2O_2. Heterogeneous reaction of SO_2 on dust is also an important uptake process [*Dentener et al.*, 1996; *Song and Carmichael*, 2001]. However, we do not include the sulfur cycle in this study. Our results on heterogeneous uptake on dust for some species should be considered an upper bound on dust uptake since some of these species would be lost to heterogeneous reactions on other aerosol types.

Using the method of *Schwartz* [1986] and *Tie et al.* [2001], the lifetime of species A associated with heterogeneous reactions on particles of radius R_p is provided by the inverse of the pseudo first-order heterogeneous rate constant k for diffusive and kinetic transport of A to the particle surface:

$$k(\mathrm{A}, R_p, T) = S[R_p/D_\mathrm{A} + 4/(v_\mathrm{A}\gamma)]^{-1} \qquad (1)$$

Here, v_A is the mean molecular speed of gas species A at temperature T [K]. We will discuss the T-dependence of k more thoroughly later in this section. D_A is the gas-phase diffusion coefficient of species A in air, and ranges from 1–2×10^{-5} m^2 s^{-1} for most species [*Schwartz*, 1986; *Pruppacher and Klett*, 1998]. Measurements of D_A have not been reported for many species modeled here, so we set $D_\mathrm{A} = 10^{-5}$ m^2 s^{-1} for all species as in *Tie et al.* [2001]. S [m^2 m^{-3}] is the surface area density of the particles and is determined from the predicted mass mixing ratio of dust in four size bins using the specific area $\underline{\mathrm{S}}$ [m^2 kg^{-1}] shown in Table 2 of *Zender et al.* [2002]. γ is the mass uptake coefficient of species A.

The uptake coefficients of the eight species considered to undergo irreversible reactions on mineral dust surfaces in our model are summarized in Table 2. Uncertainties in γ are large, up to three orders of magnitude for certain species [*Zhang and Carmichael*, 1999; *Goodman et al.*, 2000; *Michel et al.*, 2002; *Underwood et al.*, 2002]. For example, recent studies report $2.0 \times 10^{-6} < \gamma < 2.5 \times 10^{-3}$ for O_3 [*Dentener et al.*, 1996; *Michel et al.*, 2002] and $2.0 \times 10^{-5} < \gamma < 1.6 \times 10^{-2}$ for HNO_3 [*Goodman et al.*, 2000; *Underwood et al.*, 2002]. We apply the values in Table 2 globally so that regional differences in γ due to dust mineralogy and RH are neglected.

Figures 4 and 5 show the reduction of O_3 [ppb] and OH [%], respectively, due to heterogeneous reactions on dust. Since the net uptake is irreversible, mineral dust uptake reduces O_3 and OH globally. The correlation between the heterogeneous uptake of O_3 by dust (Figure 4) and the spatial distribution of dust (Figure 5 in *Zender et al.* [2002])

Table 2. Uptake Coefficients of Mineral Dust in UCI CTM

Reaction	Uptake γ	References[a]
$H_2O_2 + \text{Dust} \longrightarrow \text{Products}$	1.0×10^{-4}	1
$HNO_3 + \text{Dust} \longrightarrow \text{Products}$	1.1×10^{-3}	1, 2, 5
$HO_2 + \text{Dust} \longrightarrow \text{Products}$	0.1	1, 6
$N_2O_5 + \text{Dust} \longrightarrow \text{Products}$	1.0×10^{-3}	1, 2
$NO_2 + \text{Dust} \longrightarrow \text{Products}$	4.4×10^{-5}	5
$NO_3 + \text{Dust} \longrightarrow \text{Products}$	0.1	4, 6
$O_3 + \text{Dust} \longrightarrow \text{Products}$	5.0×10^{-5}	1, 2, 6, 3
$OH + \text{Dust} \longrightarrow \text{Products}$	0.1	6

[a]*References:* 1, *Dentener et al.* [1996]; 2, *DeMore et al.* [1997]; 3, *Michel et al.* [2002]; 4, *Seinfeld and Pandis* [1997]; 5, *Underwood et al.* [2002]; 6, *Zhang and Carmichael* [1999];

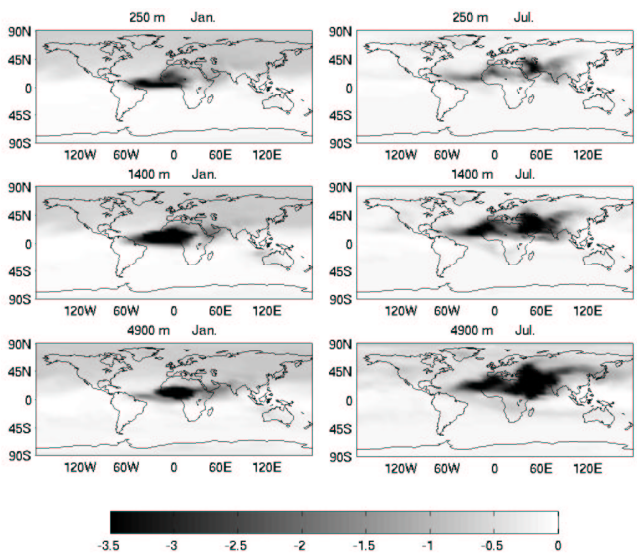

Figure 4. Decrease in O_3 [ppb] due to heterogeneous reactions on dust in January and July at three atmospheric layers.

is clear in the tropics and NH subtropics. Heterogeneous uptake of O_3 by dust is also correlated to O_3 abundance (Figure 3) except near Antarctica. In January, the maximum reduction occurs along the plume from western Africa to the tropical Atlantic ocean just above the boundary layer. In our simulations African dust that is lifted above the boundary layer in January is conveyed over the Atlantic ocean in a layer between 1–3 km known as the Saharan Air Layer (SAL) [*Karyampudi et al.*, 1999]. The O_3 change is greatest near the top of the boundary layer where the local maxima

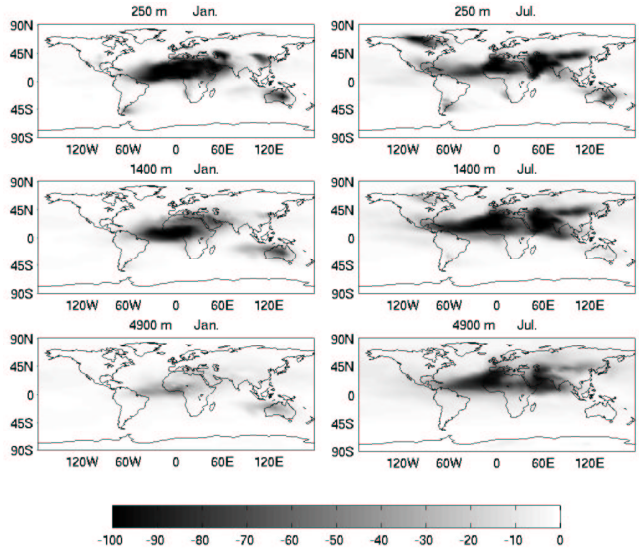

Figure 5. Decrease in OH [%] due to heterogeneous reactions on dust in January and July at three atmospheric layers.

in O_3 abundance (Figure 3) coincides with the SAL. In contrast to the photochemical response of O_3 to dust (Plate 1) in July, the O_3 response to heterogeneous uptake increases with altitude, especially over Asia. In Summer, continental low pressure cells form over north America and more deeply over Asia. The strong summertime Tibetan low pressure cell facilitates convective transport and displaces the region of heterogeneous uptake to higher altitudes over Asia.

Figure 5 shows that heterogeneous chemistry is important for OH over the high dust loading regions in both January and July, consistent with the OH photolytic perturbation. Comparing to the O_3 heterogeneous perturbation, perturbation of OH favors the lower altitudes. This reflects the quicker response of OH to indirect effects. The gas phase lifetime is only seconds for OH but is over ten days for O_3.

Table 3 lists the mean January, July, and annual changes in O_3 [%] and OH [%] due to heterogeneous chemistry on dust. Globally, O_3 decreases 0.9% and OH decreases nearly 10%. Regional reductions reach 8.5% for O_3 at the top of boundary layer over west Africa and the tropical Atlantic ocean in January and in the middle troposphere over the Arabian desert in July. OH decreases by up to 100% within the boundary layer in the zonally extensive tropical region from northern Africa to the Atlantic ocean in January and from India to the Caribbean in July. The larger chemical perturbation occurs in the NH, where trace gas reductions are more than triple those in the SH. Heterogeneous uptake changes global O_3 and OH about four times more than photochem-

Table 3. January, July, and Annual mean decrease [%] in NH, SH, and Global O_3 and OH due to heterogeneous reactions on dust.

Region	O_3			OH		
	Jan	Jul	Ann.	Jan	Jul	A
NH	−1.52	−1.43	−1.48	−10.97	−19.96	−16
SH	−0.46	−0.33	−0.30	−3.67	−3.11	−2
Global	−0.99	−0.88	−0.89	−7.32	−11.54	−9

istry.

Unfortunately, field measurements which could confirm or deny our findings for climatological heterogeneous uptake of oxidant species on mineral surfaces in dusty regions are scarce [*Bey et al.*, 2001]. Previous research has focused on the heterogeneous perturbation in dusty conditions. Using a global three-dimensional model, *Dentener et al.* [1996] estimated that heterogeneous uptake on dust leads to a $\sim$ 10% reduction of O_3 in dust source regions during the dustiest season. Using a box model, *Zhang and Carmichael* [1999] estimated that spring dust storms in East Asia decrease O_3 by 11–40%, NO_y (NO_3+N_2O_5+HNO_3) by 16–100%, and H_xO_y (OH+HO_2+H_2O_2) by 11–59% via heterogeneous uptake. Our simulations indicate global reductions due to heterogeneous uptake on dust of 0.9% for O_3, 3.9% for NO_y, and 5.1% for H_xO_y. Thus our global estimates are an order of magnitude less than estimates from other models during dusty conditions. These estimates are consistent since the annual mean dust concentration is about an order of magnitude less than during dusty conditions.

3.3. Photochemical and Heterogeneous Coupling

Sections 3.1–3.2 describe the photolytic and heterogeneous forcing of oxidants by dust, examining each process in isolation. We now quantify interactions between photolytic and heterogeneous forcing when those processes operate simultaneously, as in nature. We define the effects of the photochemical-only, heterogeneous-only, and coupled (photochemical plus heterogeneous) perturbations by dust as Δ_P, Δ_H, and Δ_{P+H} respectively. The degree of non-linear interaction between photochemical and heterogeneous effects of dust defines the coupling factor λ

$$\lambda = \Delta_{P+H}/(\Delta_P + \Delta_H) \tag{2}$$

Values of λ near unity indicate that the individual Δ_P and Δ_H perturbations are additive (i.e., linear). Plate 2 shows the zonal mean λ_{O_3} λ_{OH} and λ_{HNO_3} in January and July. In most remote and upper tropospheric regions, λ is near unity.

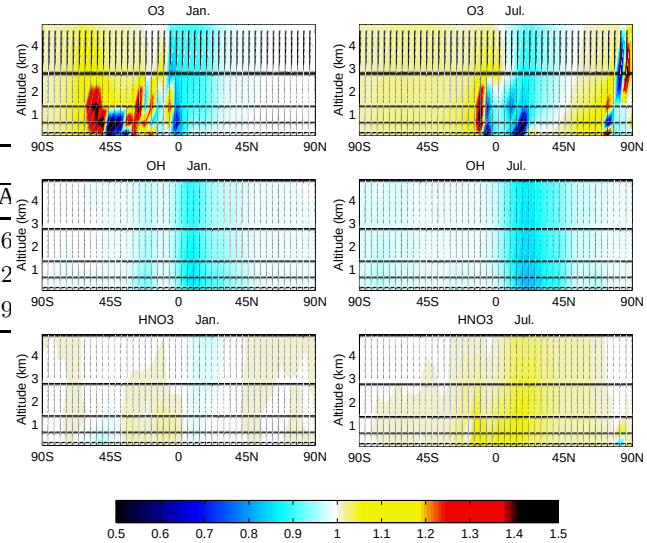

Plate 2. Zonal mean coupling factor λ between photochemical and heterogeneous effects of dust on O_3, OH, and HNO_3 in January (left column) and July (right).

In these regions, feedbacks between the photolytic and heterogeneous perturbations are generally less than 10%. The interaction increases over the subtropics, especially in the NH, where most dust resides. The involvement of O_3 in photolysis alteration gives rise to the complicated structure of λ_{O_3}. Coupling amplifies O_3 reductions in most of the SH and suppresses it in the tropics and NH in January. The effect of coupling in July is similar except in the NH mid-to-high latitudes where coupling changes from a suppressing to an amplifying effect on O_3. Strong coupling occurs in the boundary layer and lower troposphere from the equator to 50S in January and in the NH subtropical boundary layer and high latitudes in July. Other species studied in this paper exhibit coupling patterns similar to OH or to HNO_3.

We now examine the relative roles of Δ_P and Δ_H in determining Δ_{P+H}, and how the vertical structure of dust affects this relationship. The relative contribution of photochemistry δ_P to Δ_{P+H}, the net species change by dust, is defined as

$$\delta_P = \frac{\Delta_P}{|\Delta_P| + |\Delta_H|} \tag{3}$$

Thus $0 < |\delta_P| < 1$ and $|\delta_P| = 0.5$ where the magnitudes of the photochemistry-only effect and the heterogeneous-only effect of dust are equal. Strictly, this definition is only valid where $\lambda = 1$. We take this definition approximately due to the weak nonlinear interaction on global scale (Plate 2). The relative contribution of heterogeneous reactions, δ_H (not shown) is defined analogously to (3). Heterogeneous uptake

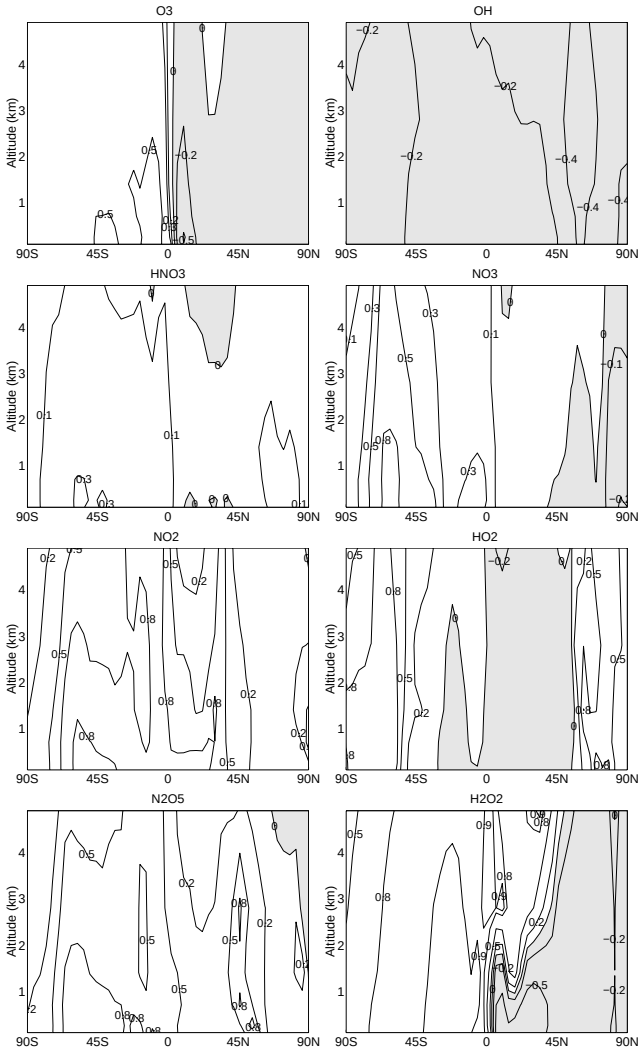

Figure 6. Relative role of photochemistry δ_{P} for eight species in Table 2 in January. Shading indicates $\delta_{\mathrm{P}} < 0$.

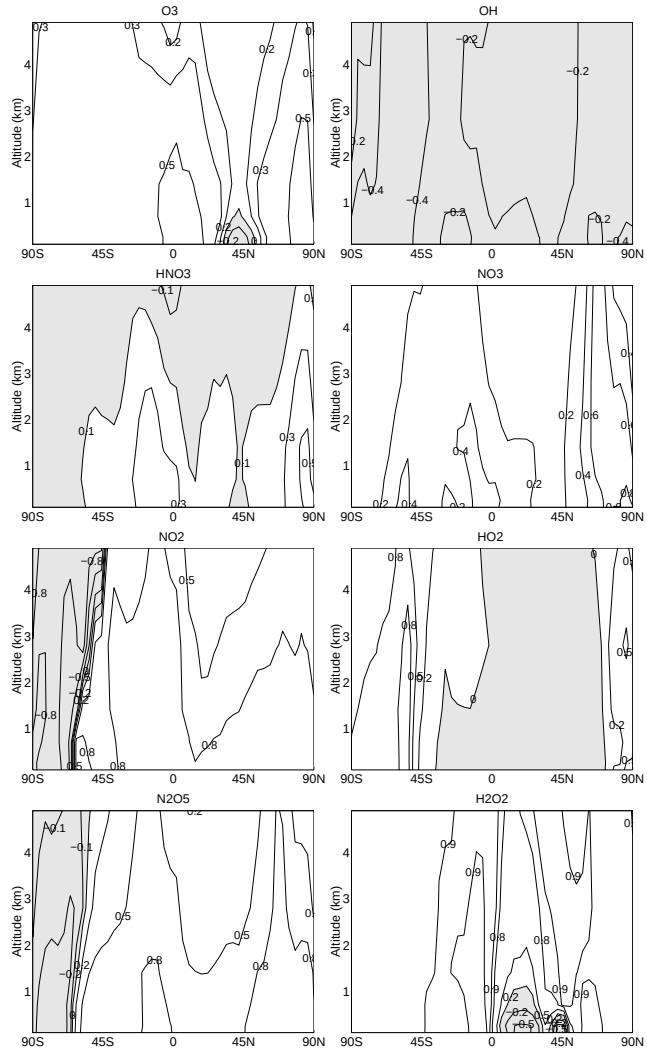

Figure 7. Same as Figure 6 except for July.

is negative definite, so that $\delta_{\mathrm{H}} \equiv -1 + |\delta_{\mathrm{P}}|$. Thus $|\delta_{\mathrm{P}}|$ is small where $|\delta_{\mathrm{H}}|$ is large, and visa versa.

Figures 6 and 7 show the zonal mean δ_{P} for the eight species in Table 2 in January and July, respectively. Most regions dominated by photolysis perturbation (i.e., $|\delta_{\mathrm{P}}| > 0.5$) are confined to low-to-mid altitudes. This is consistent with our results in the previous section that heterogeneous forcing by dust is almost four times larger than the photochemical forcing. A notable exception is $\mathrm{H_2O_2}$ for which $|\delta_{\mathrm{P}}| > |\delta_{\mathrm{H}}|$ everywhere except in the NH during January. Patterns of δ_{P} for $\mathrm{O_3}$, odd-nitrogen, and $\mathrm{N_2O_5}$ are similar. All show large values in the SH mid-latitude boundary layer in January and in tropics and the NH high latitudes in July. Among these species, $\mathrm{NO_2}$ and $\mathrm{N_2O_5}$ are most impacted by photolysis, with extensive vertical and meridional regions of large $|\delta_{\mathrm{P}}|$. Odd-hydrogen (OH and $\mathrm{HO_2}$) shows large $|\Delta_{\mathrm{P}}|$ in polar regions in both seasons.

Table 4 summarizes the annual mean changes due to photochemical-only Δ_{P}, heterogeneous-only Δ_{H}, and the coupled forcing of dust, $\Delta_{\mathrm{P+H}}$. The NH change dominates the SH change for most species, in accord with the hemispheric asymmetry of dust mass. Global annual mean tropospheric $\mathrm{O_3}$, $\mathrm{H_2O_2}$, $\mathrm{NO_2}$, and $\mathrm{N_2O_5}$ change less than or around 1%; $\mathrm{HNO_3}$, $\mathrm{HO_2}$, and $\mathrm{NO_3}$ change 3–6%, and OH changes by -11.1%. OH and $\mathrm{HO_2}$ are the most sensitive species in our study because photochemical and heteroge-

Table 4. Annual mean changes [%] of eight species due to effects of dust. Shown are Δ_P, Δ_H, and Δ_{P+H} in NH, SH, Global mean, and North Africa and the Tropical Atlantic (NATA) region downwind (80W–30E, 0–30N), and global mean and NATA-region coupling factors λ (2).

	Photolysis Δ_P				Heterogeneous Δ_H				Coupled Δ_{P+H}				λ	
	NH	SH	Global	NATA	NH	SH	Global	NATA	NH	SH	Global	NATA	Global	NATA
O_3	0.2	0.3	0.2	0.9	−1.5	−0.3	−0.9	−5.0	−1.3	−0.0	−0.7	−3.8	1.00	0.93
OH	−4.0	−0.8	−2.4	−15.0	−16.4	−2.9	−9.6	−64.0	−18.5	−3.6	−11.1	−66.8	0.93	0.85
HNO_3	0.4	0.3	0.3	0.8	−6.1	−1.5	−3.8	−28.3	−5.8	−1.2	−3.5	−27.7	1.00	1.01
HO_2	−1.0	0.2	−0.4	−6.0	−9.1	−1.1	−5.1	−43.5	−9.6	−0.9	−5.2	−45.3	0.95	0.92
NO_3	1.9	0.8	1.3	5.4	−10.2	−1.5	−5.9	−47.2	−8.7	−0.8	−4.7	−44.2	1.02	1.06
NO_2	2.1	0.7	1.4	9.8	−0.5	−0.2	−0.3	−6.9	1.6	0.5	1.1	3.1	1.00	1.07
N_2O_5	3.3	1.2	2.2	12.0	−3.4	−0.8	−2.1	−19.6	−0.3	+0.4	0.0	−9.4	—	1.24
H_2O_2	0.3	0.7	0.5	−0.6	−0.4	0.1	−0.2	−2.2	−0.2	0.8	0.3	−3.0	1.00	1.07

neous forcing by dust both decrease their abundance. In contrast, the individual changes Δ_P and Δ_H are of opposite signs for O_3, odd-nitrogen, N_2O_5, and H_2O_2. Thus cancellation by opposing responses to dust results in smaller net changes Δ_{P+H} for these species.

Table 4 also lists the global mean coupling factors λ (2). In the global mean, OH is the most sensitive to coupling—7% of its change is due to the interaction of the photochemical and heterogeneous responses to dust forcing. O_3 exhibits no sensitivity to coupling ($\lambda_{O_3} = 1$) in the global mean due to mutual cancellation of regions of positive and negative coupling (Plate 2). Thus caution is mandated in neglecting either the photochemical or heterogeneous influence of dust on O_3 on regional scales.

Finally, we examine the effects of dust on atmospheric chemistry in a dust-dominated region. This is the northern Africa and the tropical Atlantic region downwind (80W–30E,0–30N), which has the largest dust burden on the planet due to African dust sources [*Luo et al.*, 2002]. Figure 8 shows the seasonal cycles of the dust forcing (Δ_P, Δ_H, and Δ_{P+H}) of each species in Table 2. The maximum photochemical perturbation occurs during spring and summer, the chemically active season in this region. This seasonal change is also consistent with regional seasonality of dust burden from observations [*Savoie et al.*, 1992; *Holben et al.*, 1998] and simulations [*Ginoux et al.*, 2001; *Zender et al.*, 2002]. As expected the net dust perturbation on atmospheric chemistry is substantially larger in this region (see Table 4) than in the global mean. For instance, OH reduction in this region reaches −66.8%, six times the global mean OH change. Table 4 shows that the influence of photochemical-heterogeneous coupling are much stronger in the NATA region than in the global mean. Coupling accounts for 7%, 15%, and 24% of the change of O_3, OH, and N_2O_5, respectively, in the NATA region.

Our results are consistent with previous regional studies of dust-chemistry interactions in Asia. *Zhang et al.* [1994]

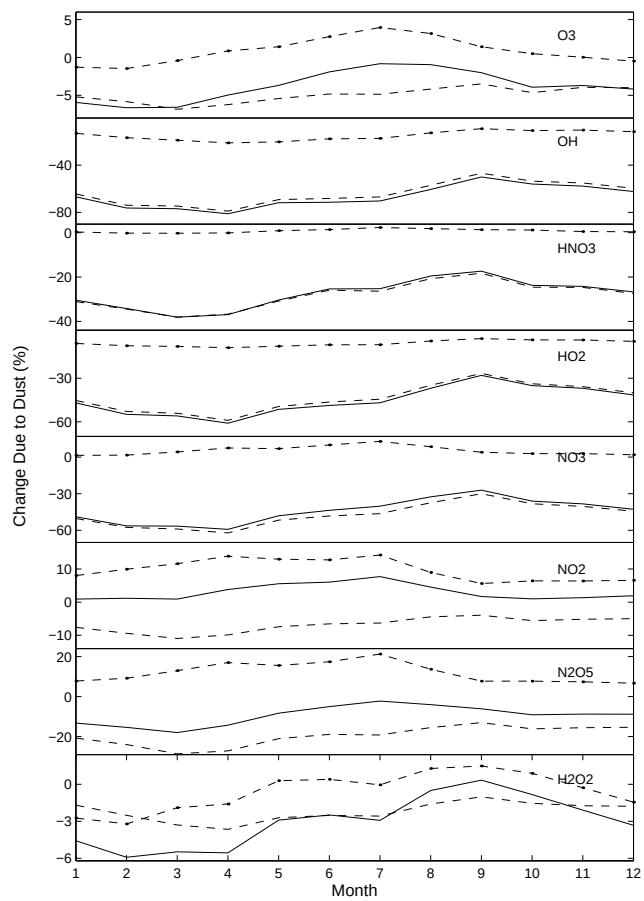

Figure 8. Seasonal cycle of chemical changes in north Africa and tropical Atlantic region downwind (80W–30E,0–30N). Shown are photochemical-only Δ_P (dot-dash), heterogeneous-only Δ_H (dash), and coupled Δ_{P+H} (solid) effects of dust.

observed short term anti-correlations of O_3 and dust concentrations in Happo, Japan. They estimated O_3 decreases about 3–10% per 10 μg m^{-3} dust. Our simulated annual mean boundary layer dust concentration in Happo, Japan is about 1.2 μg m^{-3} [*Zender et al.*, 2002]. We estimate $\Delta_{P+H}O_3$ is about -1.2% in fall, -1.3% in winter, and -1.5% in spring (consistent with *Zhang et al.*), and $+0.4\%$ in summer.

Tabazadeh et al. [1998] proposed that heterogeneous chemistry on mineral dust and biomass burning aerosols irreversibly removes gaseous HNO_3, and that representing this would reduce common model high biases in HNO_3. For example, previous studies of the nitrogen cycle simulated summertime HNO_3 levels 2–10 times larger than observed in the upper troposphere over the East China coast [*Hauglustaine et al.*, 1998; *Wang et al.*, 1998b]. The UCI CTM summertime HNO_3 bias in this region is also close to a factor of two. We find that dust reduces HNO_3 by about 60% in the mid-to-upper troposphere in and downwind of dust source regions in summer, as well as about 40% in winter. Therefore, dust only partially explains HNO_3 biases identified in *Tabazadeh et al.* [1998].

3.4. Sensitivity to Dust Spatial Distribution

In this section we examine the sensitivity of column ozone change to dust horizontal, vertical, and geographic distribution. Our goal here is to link the efficiency with which dust alters important oxidants like O_3 to physical processes, so that we understand where and why oxidants are most sensitive to marginal changes in dust emissions. We define the net O_3 forcing efficiency of dust ϵ_{P+H} as the change in tropospheric column O_3 [%] normalized by the column mass path of dust in mg m^{-2}. The analogous forcing efficiencies due to photochemistry-only and heterogeneous-only forcing are ϵ_P and ϵ_H.

Figure 9a shows the zonal mean column dust burden [mg m^{-2}] in July. The vertical scale is logarithmic and conceals the dramatic variation of dust with latitude. Figure 9b shows the July change in tropospheric O_3 [%] due to the photochemical-only and the heterogeneous-only effects of dust. Figure 9c shows the forcing efficiencies ϵ_P and ϵ_H (i.e., the ratio of panel b to panel a). Note the scale is logarithmic. Both ϵ_P and ϵ_H increase toward high latitudes, becoming several times larger in polar regions than in the NH subtropics. Thus O_3 change is far greater in remote regions, per unit local column dust mass, than in source regions. At first glance it appears that a small amount of dust transported to polar regions causes an inordinate change in polar O_3. However, this depends on whether O_3 change at high latitudes is due to local dust or to the advection of perturbed O_3 from dustier regions.

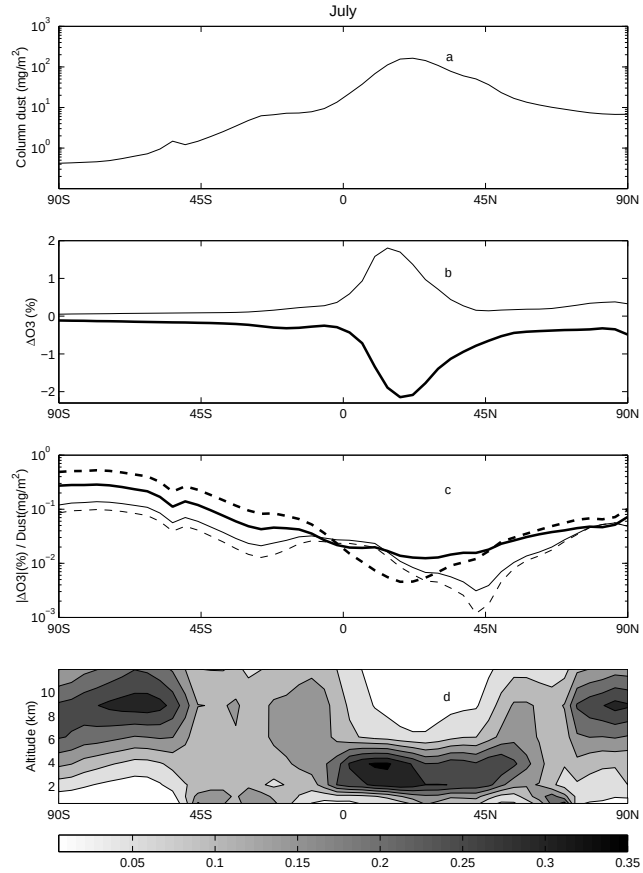

Figure 9. July zonal mean (a) column dust burden [mg m^{-2}], (b) tropospheric O_3 change [%] due to normal dust distribution broken down into Δ_P (thin line) and Δ_H (thick line), (c) O_3 forcing efficiencies of dust by photochemistry ϵ_P (thin line) and heterogeneous uptake ϵ_H (thick line). Dashed lines show corresponding $\tilde{\epsilon}_P$ and $\tilde{\epsilon}_H$ for the inverted dust distribution. (d) Normalized vertical distribution of dust.

In July, total dust burden decreases monotonically away from the NH subtropical source region (Figure 9a). The O_3 forcing peaks in the NH subtropics with slight variations in the other latitudes (Figure 9b). To determine the relative importance of transport and local chemistry in the polar regions, we diagnosed separately the advective and local chemical contributions to the O_3 budget in the region $72°$–$90°$N. In our gas-phase-only simulation, horizontal advection is an order of magnitude more important than the local chemistry in determining O_3. With dust, the change of O_3 in this region due to horizontal advection is about five times more than the change from local chemistry. Thus O_3 change in non-dusty Northern high latitudes is controlled by

transport of perturbed O_3 from the NH subtropics. Consequently, O_3 change at high latitudes appears to be insensitive to model biases in high latitude dust.

The strong meridional gradient in ϵ_P is also a function of the meridional gradient in the vertical structure of dust. Figure 9d shows the normalized vertical structure of dust. This is obtained by dividing the dust column path by the local mass path (so the values in each column sum to unity). Dust in source regions is concentrated in the lower troposphere in July (cf. Figure 1b). At the same time, dust reaching the remote high latitudes is concentrated in the upper troposphere where scavenging processes for these clay-sized ($D < 2.5$ μm) particles inefficient [*Zender et al.*, 2002]. Thus the vertical structure of dust is inverted during transport from source regions to high latitudes.

We studied the sensitivity of ozone forcing to the vertical distribution of dust by inverting the vertical profile of the dust while fixing the total dust column amount. In this sensitivity study, therefore, high-latitude dust is concentrated near the surface, while NH subtropical dust is concentrated in the upper troposphere. Figure 9c shows both the photochemical and heterogeneous forcing efficiencies derived from the realistic dust vertical distribution, ϵ_P and ϵ_H, and the efficiencies of the inverted dust distribution, $\tilde{\epsilon}_P$ and $\tilde{\epsilon}_H$. The significant separation between ϵ_P and $\tilde{\epsilon}_P$ (the scale is logarithmic), as well as between ϵ_H and $\tilde{\epsilon}_H$, shows the strong vertical sensitivity of the O_3 forcing efficiency.

Dust high in the atmosphere alters column O_3 through photolysis more than the same amount of dust in the lower atmosphere. However, $\tilde{\epsilon}_P < \epsilon_P$ in the NH subtropics. As discussed in Section 3.1, dust in low-NO_x environments increases O_3 by reducing photochemical destruction of O_3. In the normal dust vertical distribution, lower tropospheric dust from northern Africa lies beneath the mid-to-upper tropospheric NO_x from southern African biomass burning regions, resulting in increased O_3 in the dusty region. In the inverted dust scenario, upper tropospheric dust mixed with high-NO_x reduces photolytic O_3 there.

The largest discrepancy between ϵ_P and $\tilde{\epsilon}_P$ occurs near $45°$N. Dust near $45°$N that normally resides between 2–4 km is located between 5–8 km in the inverted experiment. European emissions of O_3 precursors in NH summer create a strong O_3 band in the Eurasian mid-latitudes near 5 km (Figure 3). In the inverted dust experiment, dust in the high-NO_x Eurasian mid-troposphere causes substantial O_3 reductions there. The negative O_3 change over land cancels the positive O_3 change over ocean resulting in a small zonal mean $\tilde{\epsilon}_H$ near $45°$N. The difference between ϵ_P and $\tilde{\epsilon}_P$ generally keeps constant or weakens toward the poles. Thus O_3 change in remote regions is more sensitive to global O_3 transport than to dust vertical structure.

The difference between ϵ_H and $\tilde{\epsilon}_H$ tracks the normalized dust distribution in Figure 9d. Where dust normally resides in the lower troposphere, $\epsilon_H > \tilde{\epsilon}_H$, and visa versa. In the troposphere, inverting the dust has little effect on the amount of O_3 the dust is exposed to because the zonal mean vertical distribution of O_3 is relatively homogeneous. Thus the discrepancy between ϵ_H and $\tilde{\epsilon}_H$ is largely explained by the increase of heterogeneous uptake with temperature, $v_A \propto \sqrt{T}$ in (1).

In a box model study, *He and Carmichael* [1999] reported that surface O_3 decreases slightly by dust photochemical forcing when the aerosol layer is raised within the boundary layer, but that O_3 stops changing as the aerosol layer is raised further. Our results indicate that in the real atmosphere the sensitivity of O_3 to the vertical location of dust is more complicated than this and can change signs depending on the presence of O_3 precursors. We find that in dusty regions, O_3 is sensitive not only to the height of the dust layer, but also to NO_x availability. In remote regions O_3 transport is more important than local dust vertical structure.

4. Conclusions

We simulated and analyzed the influence of mineral dust on tropospheric chemistry through its impact on atmospheric photolysis and heterogeneous chemistry. The global annual mean change due to dust is on the order of several percent for most species considered, except for OH (-11.1%). As expected the largest changes occurred in and downwind of dust source regions, e.g., northern Africa, the tropical Atlantic, and the Arabian peninsula. The changes in O_3 and OH due to dust are more than five times greater in the NH than the SH.

Photochemical and heterogeneous chemistry forcing by dust are weakly coupled in the global mean, and moderately coupled over high dust loading regions. In northern Africa and the tropical Atlantic downwind, coupling accounts for 24%, 15%, and 7% of the changes in N_2O_5, OH, and O_3, respectively. Studies which neglect photochemical-heterogeneous coupling in dusty regions are likely to have biases. Globally, heterogeneous uptake weakly modifies the atmospheric photolysis field by reducing tropospheric O_3, but this has no significant impact on photochemistry. Photochemistry generally produces more O_3, but the uptake of this additional O_3 is a second order effect.

Dust horizontal and vertical distributions influence column ozone in subtle ways. High latitude O_3 change is dominated by transport of O_3 altered by dust close to source regions. Therefore, uncertainties in dust concentration near the poles do not propagate to O_3 changes. In dusty regions, the photochemical forcing efficiency of O_3 by dust is not

only sensitive to the vertical structure of dust, but also to the coincidence of O_3 precursors. In remote regions O_3 photolytic forcing is not sensitive to dust vertical structure. The heterogeneous uptake efficiency of O_3 by dust is sensitive to the vertical structure of dust, mainly through the influence of temperature on uptake rates.

There are many uncertainties in our results. Although we adopt a widely used dust size range (0.1–10 μm) [e.g., *Joussaume*, 1990; *Tegen and Fung*, 1994; *Lohmann et al.*, 1999], our size distribution under-represents larger particles [*Zender et al.*, 2002] since nontrivial quantities of particles $D > 10$ μm have been found in and downwind dust source regions [*Li-Jones and Prospero*, 1998; *Reid et al.*, 2003]. A given mass of large particle has a smaller influence on photochemical and heterogeneous forcing than the same mass of smaller particles. On the other hand, larger particles have shorter atmosphere lifetimes so climatological errors may be small. *Zhang and Carmichael* [1999] show that most nitrate and sulfate is found on dust particles in the $1.5 < D < 10$ μm range.

The uncertainty in our estimates of the photochemical forcing of mineral dust stems from the choice of refractive index n compounded by regional biases in the size and vertical distribution [*Bian et al.*, 2002]. Previous studies show that dust strongly absorbs in the near ultraviolet, and that n varies with wavelength [*Savoie et al.*, 2000; *Diaz et al.*, 2001; *Kaufman et al.*, 2001; *Dubovik et al.*, 2002]. Although the constant dust refractive index adopted in this study (Section 3.1) results in high dust absorption at key tropospheric photochemical wavelengths (300–400 nm), it should have a strong wavelength dependence.

The uptake coefficients in Table 2 are taken to be globally uniform, although the mineralogical composition of dust varies with sources [*Sokolik et al.*, 2001; *Michel et al.*, 2002]. Uptake coefficients may also very with Relative Humidity. For example, γ_{HNO_3} would be significantly increased with RH increase, while the effect of absorbed water on γ_{NO_2} is less clear [*Underwood et al.*, 2002]. However, $\gamma(\mathrm{RH})$ for interesting species is currently unknown.

Due to these uncertainties in model inputs, this study should be regarded as exploratory and subject to further improvements, including improved model evaluation. Unfortunately, field data to evaluate modeled dust photochemical and heterogeneous effects are limited. Few comprehensive measurements of O_3 have been performed in dusty regions, and the available observations, being for limited field experiments, do not provide representative climatologies. Records for other photochemically active species are also sparse. Recent field campaigns such as ACE-Asia and ITCT 2k2 will greatly facilitate future studies since these campaigns were conducted in and downwind of dust source region during Asian dust outbreaks. Fully evaluating the seasonality, geographic location, and vertical structure of dust perturbation predicted by our model, however, will require sustained measurements in dusty regions.

Acknowledgments. We thank M. Prather for helpful comments. P. Jöeckel provided code to re-grid netCDF data. This research was supported by NASA Grants NAG5-10147 and NAG5-10546.

References

Atkinson, R., D. Baluch, R. Cox, R. Hampson, J. Kerr, and M. Troe, Evaluated kinetic, photochemical and heterogeneous data for atmospheric chemistry: Supplement V — IUPAC Subcommittee on Gas Kinetic Data Evaluation for Atmospheric Chemistry, *J. Phys. Chem. Ref. Data*, *26*, 521–1011, 1997.

Balis, D. S., C. S. Zerefos, K. Kourtidis, A. F. Bais, A. Hofzumahaus, A. Kraus, R. Schmitt, M. Blumthaler, and G. P. Gobbi, Measurements and modeling of photolysis rates during the PAUR II campaign, *Submitted to J. Geophys. Res.*, 2001.

Baughcum, S., T. Tritz, S. Henderson, and D. Pickett, Scheduled civil aircraft emission inventories for 1992: Database development and analysis, *Tech. Rep. Tech. rept. NASA CR-4700*, 1996.

Bey, I., D. J. Jacob, J. A. Logan, and R. M. Yantosca, Asian chemical outflow to the pacific in spring: Origins, pathways, and budgets, *J. Geophys. Res.*, *106*, 23097–23113, 2001.

Bian, H., and M. J. Prather, Fast-J2: Accurate simulation of stratospheric photolysis in global chemistry models, *J. Atmos. Chem.*, *41*, 281–296, 2002.

Bian, H., M. Prather, and T. Takemura, The influences of aerosols on tropospheric photolysis and tracers global budgets, *To be submitted to J. Geophys. Res.*, 2002.

Carver, G. D., P. D. Brown, and O. Wild, The ASAD atmospheric chemistry integration package and chemical reaction database, *Comput. Phys. Commun.*, *105*, 197–215, 1997.

Collins, W. D., P. J. Rasch, B. E. Eaton, B. Khattatov, J.-F. Lamarque, and C. S. Zender, Forecasting aerosols using a chemical transport model with assimilation of satellite aerosol retrievals: Methodology for INDOEX, *J. Geophys. Res.*, *106*, 7313–7336, 2001.

Collins, W. D., P. J. Rasch, B. E. Eaton, D. W. Fillmore, J. T. Kiehl, C. T. Beck, and C. S. Zender, Simulation of aerosol distributions and radiative forcing for INDOEX: Regional climate impacts, *In Press in J. Geophys. Res.*, 2002.

DeMore, W. B., S. P. Sander, D. M. Golden, R. F. Hampson, M. J. Kurylo, C. J. Howard, A. R. Ravishankara, C. E. Kolb, and M. J. Molina, Chemical kinetics and photochemical data for use in stratospheric modeling, *Evaluation Number 12 97-4*, Jet Propulsion Laboratory, Pasadena Calif., 1997.

Dentener, F. J., G. R. Carmichael, Y. Zhang, J. Lelieveld, and P. J. Crutzen, Role of mineral aerosol as a reactive surface in the global troposphere, *J. Geophys. Res.*, *101*, 22869–22889, 1996.

Diaz, J., F. Exposito, C. Torres, F. Herrera, J. Prospero, and M. Romero, Radiative properties of aerosols in Saharan dust outbreaks using ground-based and satellite data: Applications to radiative forcing, *J. Geophys. Res.*, *106*, 18403–18416, 2001.

Dickerson, R. R., S. Kondragunta, G. Stenchikov, K. L. Civerolo, B. G. Doddridge, and B. N. Holben, The impact of aerosols on solar ultraviolet radiation and photochemical smog, *Science*, *278*, 827–830, 1997.

Dubovik, O., B. Holben, T. F. Eck, A. Smirnov, Y. J. Kaufman, M. D. King, D. Tanré, and I. Slutsker, Variability of absorption and optical properties of key aerosol types observed in worldwide locations, *J. Atmos. Sci.*, *59*, 590–608, 2002.

Galy-Lacaus, C., C. R. Carmichael, C. H. Song, J. P. Lacaux, H. A. Ourabi, and A. I. Modi, Heterogeneous processes involving nitrogenous compounds and Saharan dust inferred from measurements and model calculations, *J. Geophys. Res.*, *91*, 12559–12578, 2002.

Ginoux, P., M. Chin, I. Tegen, J. Prospero, B. Holben, O. Dubovik, and S.-J. Lin, Sources and distributions of dust aerosols simulated with the GOCART model, *J. Geophys. Res.*, *106*, 20555–20273, 2001.

Goodman, A. L., G. M. Underwood, and V. H. Grassian, A laboratory study of the heterogeneous reaction of nitric acid on calcium carbonate particles, *J. Geophys. Res.*, *105*, 29053–29064, 2000.

Hauglustaine, D. A., G. P. Brasseur, S. Walters, P. J. Rasch, J.-F. Müller, L. K. Emmons, , and M. A. Carroll, MOZART, a global chemical transport model for ozone and related chemical tracers 2. Model results and evaluation, *J. Geophys. Res.*, *103*, 28291–28335, 1998.

He, S., and G. R. Carmichael, Sensitivity of photolysis rates and ozone production in the troposphere to aerosol properties, *J. Geophys. Res.*, *104*, 26307–26324, 1999.

Holben et al., B. N., AERONET – a federated instrument network and data archive for aerosol characterization, *Remote Sens. Environ.*, *66*, 1–16, 1998.

Hough, A., Development of a two-dimensional global tropospheric model: Model chemistry, *J. Geophys. Res.*, *96*, 7325–7362, 1991.

Jacobson, M., Studying the effects of aerosols on vertical photolysis rate coefficient and temperature profiles over an urban airshed, *J. Geophys. Res.*, *103*, 10593–10604, 1998.

Joussaume, S., Three-dimensional simulations of the atmospheric cycle of desert dust particles using a general circulation model, *J. Geophys. Res.*, *95*, 1909–1941, 1990.

Karyampudi, V. M., et al., Validation of the Saharan dust plume conceptual model using lidar, Meteosat, and ECMWF data, *Bull. Am. Meteorol. Soc.*, *80*, 1045–1075, 1999.

Kaufman, Y., D. Tanre, O. Dubovik, A. Karnieli, and L. Remer, Absorption of sunlight by dust as inferred from satellite and ground-based remote sensing, *Geophys. Res. Lett.*, *28*, 1479–1482, 2001.

Li-Jones, X., and J. M. Prospero, Variations in the size distribution of non-sea-salt sulfate aerosol in the marine boundary layer at Barbados: Impact of African dust, *J. Geophys. Res.*, *103*, 16073–16084, 1998.

Li-Jones, X., H. B. Maring, and J. M. Prospero, Effect of relative humidity on light scattering by mineral dust aerosol as measured in the marine boundary layer over the tropical Atlantic Ocean, *J. Geophys. Res.*, *103*, 31113–31121, 1998.

Liao, H., and J. H. Seinfeld, Radiative forcing by mineral dust aerosols: sensitivity to key variables, *J. Geophys. Res.*, *103*, 31637–31645, 1998.

Lohmann, U., J. Feichter, C. C. Chuang, and J. E. Penner, Prediction of the number of cloud droplets in the ECHAM GCM, *J. Geophys. Res.*, *104*, 9169–9198, 1999.

Luo, C., N. M. Mahowald, C. S. Zender, and J. del Corral, A 22-year climatology of mineral aerosols, *Submitted to Tellus*, 2002.

Mahowald, N. M., C. S. Zender, C. Luo, D. Savoie, O. Torres, and J. del Corral, Understanding the 30 year barbados desert dust record, *In Press in J. Geophys. Res.*, 2002.

McLinden, C. A., S. C. Olsen, B. Hannegan, O. Wild, M. J. Prather, and J. Sundet, Stratospheric ozone in 3-d models: A simple chemistry and the cross-tropopause flux, *J. Geophys. Res.*, *105*, 14653–14665, 2000.

Michel, A. E., C. R. Usher, and V. H. Grassian, Heterogeneous and catalytic uptake of ozone on mineral oxides and dust: A Knudsen cell investigation, *Submitted to Geophys. Res. Lett.*, 2002.

Murphy, D. M., and D. W. Fahey, An estimate of the flux of stratospheric reactive nitrogen and ozone into the troposphere, *J. Geophys. Res.*, *99*, 5325–5332, 1994.

Olson, J., et al., Results from the Intergovernmental Panel on Climatic Change Photochemical Model Intercomparison (Photo-Comp), *J. Geophys. Res.*, *102*, 5979–5991, 1997.

Park, J., M. Ko, C. Jackman, and R. Plumb, Models and measurements II, *Tech. Rep. Tech. rept.*, 1999.

Patterson, E. M., Optical properties of the crustal aerosol: Relation to chemical and physical characteristics, *J. Geophys. Res.*, *86*, 3236–3246, 1981.

Penner, J. E., et al., Aerosols, their direct and indirect effects, in *Climate Change 2001: The Scientific Basis. Contribution of Working Group I to the Third Assessment Report of the Intergovernmental Panel on Climate Change*, edited by J. T. Houghton, Y. Ding, D. J. Griggs, M. Noguer, P. J. van der Linden, X. Dai, K. Maskell, and C. A. Johnson, chap. 5, pp. 291–336, Cambridge Univ. Press, Cambridge, UK, and New York, NY, USA, 2001.

Prather, M. J., Numberical advection by conservation of second-order moments, *J. Geophys. Res.*, *91*, 6671–6681, 1986.

Price, C., and D. Rind, A simple lightning parameterization for calculating global lightning distributions, *J. Geophys. Res.*, *97*, 9919–9933, 1992.

Pruppacher, H. R., and J. D. Klett, *Microphysics of Clouds and Precipitation*, 2nd ed., Kluwer Acad. Publ., Dordrecht, Holland, 1998.

Ram, M., and G. Koenig, Continuous dust concentration profile of pre-Holocene ice from the Greenland Ice Sheet Project 2 ice core: Dust stadials, interstadials, and the Eemian, *J. Geophys. Res.*, *102*, 26641–26648, 1997.

Rasch, P. J., N. M. Mahowald, and B. E. Eaton, Representations of transport, convection, and the hydrologic cycle in chemical transport models: Implications for the modeling of short-lived and soluble species, *J. Geophys. Res.*, *102*, 28127–28138, 1997.

Rasch, P. J., W. D. Collins, and B. E. Eaton, Understanding the Indian Ocean Experiment INDOEX aerosol distributions with an aerosol assimilation, *J. Geophys. Res.*, *106*, 7337–7355, 2001.

Reid, J. S., et al., Comparison of size and morphological measurements of coarse mode dust particles from Africa, *Submitted to J. Geophys. Res.*, 2003.

Savoie, D. L., J. M. Prospero, S. J. Oltmans, W. C. Graustein, K. K. Turekian, J. T. Merrill, and H. Levy II, Sources of nitrate and ozone in the marine boundary layer of the tropical North Atlantic, *J. Geophys. Res.*, *97*, 11575–11589, 1992.

Savoie, D. L., H. Maring, M. Izaguirre, T. Snowdon, and L. Custals, Ground-based measurements of aerosol chemical, physical, and optical properties during the Puerto Rico Dust Experiment (PRIDE), in *Eos, Transactions*, vol. 81, p. F44, American Geophysical Union, 2000.

Schwartz, S. E., Mass-transport considerations pertinent to aqueous phase reactions of gases in liquid-water clouds, in *Chemistry of Multiphase Atmospheric Systems*, edited by W. Jaeschke, vol. 6 of *NATO ASI Series G: Ecological Sciences*, pp. 415–471, Springer-Verlag, Berlin, 1986.

Seinfeld, J. H., and S. N. Pandis, *Atmospheric Chemistry and Physics*, John Wiley & Sons, New York, NY, 1997.

Sokolik, I. N., D. M. Winker, G. Bergametti, D. A. Gillette, G. Carmichael, Y. J. Kaufman, L. Gomes, L. Schuetz, and J. E. Penner, Introduction to special section: Outstanding problems in quantifying the radiative impacts of mineral dust, *J. Geophys. Res.*, *106*, 18015–18027, 2001.

Song, C., and G. Carmichael, A three-dimensional modeling investigation of the evolution processes of dust and sea-salt particles in east Asia, *J. Geophys. Res.*, *106*, 18131–18154, 2001.

Tabazadeh, A., M. Z. Jacobson, H. B. Singh, O. B. Toon, S. J. Lin, R. B. Chatfield, A. N. Thakur, R. W. Talbot, and J. E. Dibb, Nitric acid scavenging by mineral and biomass burning aerosols, *Geophys. Res. Lett.*, *25*, 4185–4188, 1998.

Tegen, I., and I. Fung, Modeling of mineral dust in the atmosphere: Sources, transport, and optical thickness, *J. Geophys. Res.*, *99*, 22897–22914, 1994.

Tegen, I., and I. Fung, Contribution to the atmospheric mineral aerosol load from land surface modification, *J. Geophys. Res.*, *100*, 18707–18726, 1995.

Tie, X., G. Brasseur, L. Emmons, L. Horowitz, and D. Kinnison, Effects of aerosols on tropospheric oxidants: A global model study, *J. Geophys. Res.*, *106*, 22931–22964, 2001.

Underwood, G. M., C. H. Song, M. Phadnis, G. R. Carmichael, and V. H. Grassian, Heterogeneous reactions of NO_2 and HNO_3 on oxides and mineral dust: A combined laboratory and modeling study, *J. Geophys. Res.*, *106*, 18055–18066, 2002.

Valero, F. P. J., S. K. Pope, B. C. Bush, Q. Nguyen, D. Marsden, R. D. Cess, A. S. Simpson-Leitner, A. Bucholtz, and P. M. Udelhofen, The absorption of solar radiation by the clear and cloudy atmosphere during the atmospheric radiation measurements enhanced shortwave experiments (ARESE) I and II: Observations and models, *Submitted J. Geophys. Res.*, 2002.

Wang, Y., D. Jacob, and J. Logan, Global simulation of tropospheric O_3-NO_x-hydrocarbon chemistry. 1. Model formulation, *J. Geophys. Res.*, *103*, 10713–10725, 1998a.

Wang, Y., J. Logan, and D. Jacob, Global simulation of tropospheric O_3-NO_x-hydrocarbon chemistry. 2. Model evaluation and global ozone budget, *J. Geophys. Res.*, *103*, 10727–10755, 1998b.

Wild, O., and H. Akimoto, Intercontinental transport of ozone and its precursors in a three-dimensional global CTM, *J. Geophys. Res.*, *106*, 27729–27744, 2001.

Wild, O., and M. J. Prather, Excitation of the primary tropospheric chemical mode in a global three-dimensional model, *J. Geophys. Res.*, *105*, 24647–24660, 2000.

Wild, O., X. Zhu, and M. Prather, Fast-J: Accurate simulation of in- and below-cloud photolysis in tropospheric chemical models, *J. Atmos. Chem.*, *37*, 245–282, 2000.

Zender, C. S., H. Bian, and D. Newman, The mineral Dust Entrainment And Deposition (DEAD) model: Description and 1990's dust climatology, *Submitted to J. Geophys. Res.*, 2002.

Zhang, Y., and G. R. Carmichael, The role of mineral aerosol in tropospheric chemistry in East Asia–a model study, *J. Appl. Meteorol.*, *38*, 353–366, 1999.

Zhang, Y., Y. Sunwoo, V. Kotamarthi, and G. R. Carmichael, Photochemical oxidant processes in the presence of dust: An evaluation of the impact of dust on particulate nitrate and ozone formation, *J. Appl. Meteorol.*, *33*, 813–824, 1994.

H. Bian, C. S. Zender, Department of Earth System Science, University of California, Irvine, CA 92697-3100. (hbian@uci.edu)

Received Month Day, 2002; revised Month Day, 2002; accepted Month Day, 2002.

This preprint was prepared with AGU's LaTeX macros v5.01, with the extension package 'AGU++' by P. W. Daly, version 1.6b from 1999/08/19.